Int J Adv Manuf Technol
DOI 10.1007/s00170-011-3835-z

ORIGINAL ARTICLE

Multiresponse optimization of laser welding of stainless steels in a constrained fillet joint configuration using RSM

M. M. A. Khan · L. Romoli · Marco Fiaschi · G. Dini · F. Sarri

Received: 21 March 2011 / Accepted: 5 December 2011

Abstract This paper presents experimental design approach to process parameter optimization for CW Nd/YAG laser welding of ferritic/austenitic stainless steels in a constrained fillet configuration. To determine the optimal welding parameters, response surface methodology was used to develop a set of mathematical models relating the welding parameters to each of the weld characteristics. The quality criteria considered to determine the optimal settings were the maximization of weld resistance length and shearing force, and the minimization of weld radial penetration. Laser power, welding speed, and incident angle are the factors that affect the weld bead characteristics significantly. A rapid decrease in weld shape factor and increase in shearing force with the line energy input in the range of 15–17 kJ/m depicts the establishment of a keyhole regime. A focused beam with laser power and welding speed respectively in the range of 860–875 W and 3.4–4.0 m/min and an incident angle of around 12° were identified as the optimal set of laser welding parameters to obtain stronger and better welds.

Keywords RSM · Optimization · Laser welding · Stainless steels

M. M. A. Khan (✉) · L. Romoli · G. Dini
Department of Mechanical, Nuclear and Production Engineering, University of Pisa,
Pisa, Italy
e-mail: muhshin.khan@ing.unipi.it

M. Fiaschi · F. Sarri
Continental Automotive Italy S.p.A.,
Pisa, Italy

1 Introduction

In recent years, interest in the use of laser welding as a joining process in various industrial applications has increased rapidly because of its associated unique features such as the low and precise heat input, small heat-affected zone, deep and narrow fusion zone, low residual stress, and weld distortion and high welding speed [1, 2]. These features come from its high-power density, which make laser welding one of the principal welding techniques [3–5]. Laser welding being autogenous needs no filler materials resulting in reduction in welding costs and increase in weld quality [6, 7]. Generally, welding quality is characterized by the weld bead geometry, which plays an important role in determining the mechanical properties of the weld [8]. To achieve a good weld quality, the influential welding process parameters such as laser beam power, welding speed, focal position, shielding gas, and focused position should be selected and controlled accurately [7, 9–11].

However, the selection of the welding parameters that would produce an excellent welded joint is the main challenge for today's manufacturers. Usually, the desired welding process parameters are determined based on a time-consuming trial and error development effort with input parameters. This approach does not ensure that the selected welding parameters result in optimal or near-optimal weld pool geometry [8]. Also, the accuracy of process parameters thus selected depends on the skill and the experience of the engineers or machine operators. To predict the welding parameters accurately, without consuming time, materials, and labor effort, various optimization methods are available

Published online: 04 January 2012

Table 1 Chemical compositions of base metals of the weld

Base metals	Chemical compositions (%Wt.)							Thermal conductivity (W/mK)
	C	Cr	Ni	Mn	P	S	Si	
AISI 304L	0.03	18.0–20.0	8.0–12.0	2.0	0.45	0.03	1.0	15–25.1
AISI 430	0.12	16.0–18.0	0.75	1.0	0.04	0.03	1.0	25–26.9

to define the desired output variables. Considering the capabilities of reducing a great number of experimental trials as compared to other approaches and developing mathematical functions to achieve a logical relationship between the input and output parameters, many researchers have been motivated to apply response surface methodology (RSM) for predicting and optimizing the welding process parameters.

Benyounis et al. [12] studied the effect of the main laser welding parameters on the weld-bead profile using RSM to develop appropriate models. The results indicated that the developed models could be used to find optimum welding conditions for the desired criteria. It was found that welding speed had a negative effect on all the responses investigated whereas the laser power had a positive effect. Besides, as the focused position went in the metal ($F<0$) the penetration significantly reduced, but weld width increased. Manonmani et al. [13] used RSM to develop mathematical models to predict the geometry of weld bead in butt joint of austenitic stainless steel AISI304 sheets. Results pointed out that the mathematical models developed for predicting weld bead geometry could be used effectively in analyzing the cause and effect of the process parameters on response. They also found that weld width, penetration depth, and area of penetration increased with an increase of beam power and decreased with an increase in welding speeding and beam angle. Benyounis et al. [14] employed RSM to relate the laser welding input parameters (laser power, welding speed, and focal position) to each of the response outputs (i.e., tensile strength, impact strength, and operating cost) and to find out the optimal welding combination that would maximize both the tensile and impact strengths while keeping the cost relatively low. The results obtained from their investigation showed that a laser power between 1.2 and 1.23 kW was an optimum input to obtain an excellent welded component and the welding speed was the most effective welding parameter and its interaction with the focal point position should be monitored. Moradi and Ghoreishi [15] developed statistical models using RSM to investigate the effect of laser butt welding parameters on the geometrical shape of Ni-base super-alloy Rene 80. They concluded that the developed models were adequate and appropriate to predict and investigate the effects of the process parameters. Welding speed was found to be the most important parameter with the reverse effect on process outputs, whereas laser power had a direct influence on all investigated responses. Padmanaban and Balasubramanian [16] developed an empirical relationship using RSM to predict tensile strength of laser beam welded AZ31B magnesium alloy joint and to find the optimal welding conditions to attain maximum tensile strength. It was found that the developed relationship could be effectively used to predict the tensile strength of laser beam welded joints at 95% confidence level. Welding speed was the factor which had the greatest influence on tensile strength, followed by laser power and focal position. Rajakumar et al. [17]

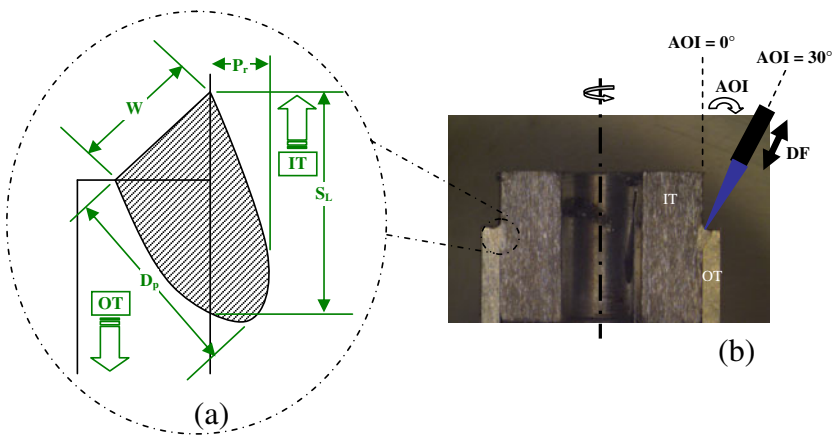

Fig. 1 Diagrams showing **a** bead characteristics of a welded fillet joint, and **b** adopted laser-welding procedure

Table 2 Experimental conditions and response factors

Process factors	Symbols	Limits				
		−2	−1	0	+1	+2
Laser power (W)	P	600	700	800	900	1,000
Welding speed (m/min)	S	2.0	3.5	3.0	3.5	4.0
Angle of incidence (°)	A	10	15	20	25	30
Defocus distance (mm)	D	−1.5	−0.75	0	+0.75	+1.5
Constant factors						
Base material	Outer tube			AISI 304L		
	Inner tube			AISI 430		
Laser source	Continuous wave			Nd/YAG laser		
Shielding gas	Type			Argon		
	Flow rate			29 l/min		
Response factors						
Weld bead characteristics	Weld penetration depth (D_p), radial penetration (P_r), and resistance length (S_L)					
Weld mechanical properties	Weld shearing force (F_s)					

developed mathematical models using RSM to analyze the effect of friction stir welding (FSW) process parameters and tool parameters on the tensile strength of AA7075 aluminum alloy. Multi-objective optimization using RSM was found to be a useful technique to optimize the friction stir welding parameters to obtain the maximum tensile strength of FSW joints. They also concluded that welding speed was the most predominant welding parameter and its interaction with the rotational speed should be monitored. Ruggiero et al. [18] studied the CW CO_2 dissimilar laser butt welding of low carbon steel and austenitic steel. They used RSM to relate laser welding input parameters to response variations and to find the optimal welding combinations. The results indicated that the proposed models predicted the responses adequately within the limits of welding parameters being used. Besides, the welding speed was the parameter that most significantly influenced the main weld bead dimensions, the middle width, and the area.

1.1 Research objectives

The welding process parameters have apparently very complex relationships with the weld bead geometry determining the mechanical properties of the weld. Welding the dissimilar metals is more complicated than that of similar metals due to difference in the physical,

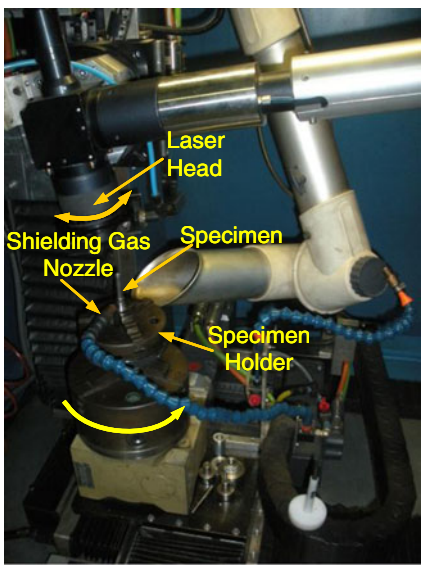

Fig. 2 Photographic view of Nd/YAG laser welding system

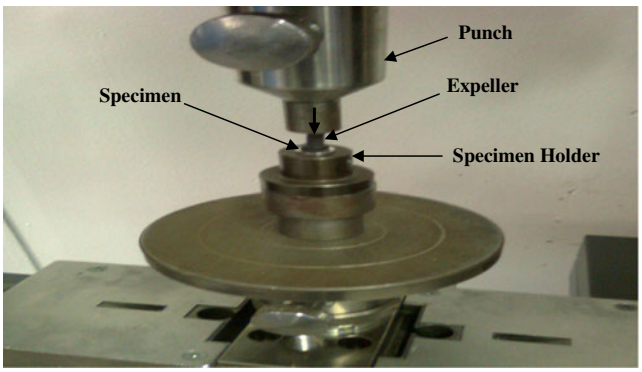

Fig. 3 Photographic view of the experimental setup for push out test

Table 3 Design matrix with actual factors and measured mean responses

Process factors				Response factors			
P (W)	S (m/min)	A (degrees)	D (mm)	S_L (mm)	P_r (mm)	D_p (mm)	F_s (kN)
700	2.5	15	−0.75	1.130	0.160	1.064	28.98
900	2.0	15	−0.75	1.337	0.240	1.368	30.84
700	3.5	15	−0.75	0.843	0.094	0.857	25.01
900	3.5	15	−0.75	1.223	0.173	1.137	28.32
700	2.5	25	−0.75	0.943	0.353	1.123	27.01
900	2.5	25	−0.75	1.150	0.466	1.390	28.56
700	3.5	25	−0.75	0.803	0.273	0.883	24.95
900	3.5	25	−0.75	0.977	0.387	1.189	26.41
700	2.5	15	0.75	1.097	0.167	1.203	27.59
900	2.5	15	0.75	1.457	0.293	1.457	31.32
700	3.5	15	0.75	0.880	0.130	0.990	25.54
900	3.5	15	0.75	1.330	0.200	1.240	29.28
700	2.5	25	0.75	0.940	0.320	0.980	26.48
900	2.5	25	0.75	1.040	0.430	1.320	27.78
700	3.5	25	0.75	0.790	0.200	0.810	24.93
900	3.5	25	0.75	0.952	0.316	1.093	27.09
600	3.0	20	0.00	0.830	0.140	0.890	25.69
1,000	3.0	20	0.00	1.370	0.380	1.590	29.54
800	2.0	20	0.00	1.360	0.350	1.470	30.85
800	4.0	20	0.00	1.040	0.200	1.030	26.88
800	3.0	10	0.00	1.030	0.140	1.120	27.89
800	3.0	30	0.00	0.800	0.475	0.989	25.42
800	3.0	20	−1.50	1.260	0.150	0.968	29.55
800	3.0	20	1.50	1.021	0.130	0.987	27.21
800	3.0	20	0.00	1.220	0.240	1.270	28.19
800	3.0	20	0.00	1.080	0.340	1.250	27.24
800	3.0	20	0.00	1.000	0.270	1.200	27.32
800	3.0	20	0.00	1.130	0.290	1.260	27.18
800	3.0	20	0.00	1.150	0.300	1.240	28.96
800	3.0	20	0.00	1.240	0.220	1.260	29.07

mechanical, and metallurgical properties of the metals to be joined. Laser welding of dissimilar ferritic and austenitic stainless steels in a circular and constrained fillet joint configuration has not been studied and reported yet. This is because this configuration complicates the joint design and inaccurate positioning of the focused beam at the corner can cause its interference with the vertical surface on its way to weld plane and reflection back to the adjacent horizontal surface making the welding process more complex. To solve the problems associated with laser welding of dissimilar ferritic and austenitic stainless steels and to obtain welds with adequate properties, it is essential to precisely select and control the welding processes and the process parameters. This paper will, therefore, try to find the optimal conditions for Nd/YAG laser beam welding of ferritic/austenitic stainless steels in fillet joint configuration. This study will focus on:

- development of empirical relationships linking the laser fillet welding input parameters (laser power, welding speed, laser beam incident angle, and defocus distance) and each of the four output responses (weld penetration depth, radial penetration, resistance length, and shearing force) using RSM,
- statistical and experimental validations of the developed models,
- determination of the optimal welding combinations that would maximize both the weld resistance length and shearing force and minimize the weld radial penetration.

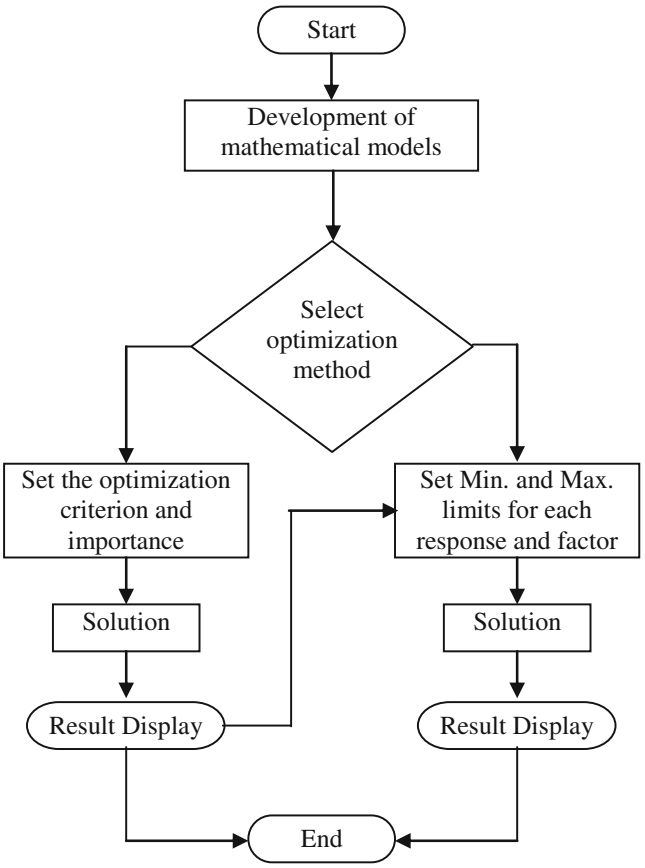

Fig. 4 Flow chart of optimization step

2 Materials and methods

2.1 Materials

Two tubular-shaped parts of ferritic AISI 430 and austenitic AISI 304 L stainless steels were fillet welded in a circular configuration to produce the welded joint. The selection of this material combination is based on both technical and economical reasons as they can provide satisfactory service performance and considerable savings, and also on their frequent use in welded form in automotive industries for making various types of fuel injectors. The chemical compositions of the base metals and the weld bead characteristics are shown in Table 1 and Fig. 1, respectively. In this study, inner and outer tubes with 2.9±0.02 and 1.75±0.02 mm wall thicknesses, respectively, are first assembled together by a clearance fit and then fillet welded autogenously.

2.2 Response surface methodology

RSM is a collection of mathematical and statistical techniques that are useful for modeling and analyzing engineering problems. In this technique, the main objective is to optimize (maximize or minimize or equal to a specific target value) the response surface that is influenced by various process parameters [19]. Fundamental to RSM is the model(s) that specify the relationships among one or more measured responses and a number of accurately controllable predictors or input factors [20]. If all the independent variables are measurable, continuous, and controllable by experiments with negligible errors, the response surface can be expressed by

$$y = f(\chi_1, \chi_2 \cdots\cdots\cdots \chi_k) \quad (1)$$

where, y is the response of the system, f is the true response function whose form is unknown and perhaps very complicated, χ_i is the variable of action called factor, and k is the number of independent variables.

In order to optimize the response "y", it is, therefore, essential to find a suitable approximation for the true functional relationship between the independent variables and the response surface [21]. The postulated mathematical

Table 5 Model summary statistics for weld penetration depth

Source	SD	R^2	Adjusted R^2	Predicted R^2	PRESS	
Linear	0.096	0.7897	0.7560	0.6956	0.34	
2FI	0.099	0.8313	0.7425	0.7156	0.31	
Quadratic	0.027	0.9899	0.9806	0.9543	0.050	Suggested
Cubic	0.024	0.9964	0.9850	0.8854	0.13	Aliased

Table 4 Sequential model sum of squares for weld penetration depth

Source	Sum of squares	*df*	Mean square	*F* value	*p* Value prob>*F*	
Mean	39.97	1	39.97			
Linear	0.870	4	0.220	23.47	<0.0001	
2FI	0.046	6	0.0076	0.78	0.5952	
Quadratic	0.170	4	0.044	59.14	<0.0001	Suggested
Cubic	0.007	8	0.0009	1.56	0.2846	Aliased

Table 6 Sequential model sum of squares for weld radial penetration

Source	Sum of squares	*df*	Mean square	*F* value	*p* Value prob>*F*	
Mean	2.04	1	2.040			
Linear	0.27	4	0.0670	29.96	<0.0001	
2FI	0.0093	6	0.0015	0.63	0.7041	
Quadratic	0.034	4	0.0085	10.12	0.0004	Suggested
Cubic	0.0015	8	0.0019	0.12	0.9964	Aliased

Table 7 Model summary statistics for weld radial penetration

Source	SD	R^2	Adjusted R^2	Predicted R^2	PRESS	
Linear	0.047	0.8274	0.7998	0.7468	0.082	
2FI	0.050	0.8561	0.7803	0.7749	0.073	
Quadratic	0.029	0.9611	0.9248	0.9005	0.032	Suggested
Cubic	0.040	0.9657	0.8578	0.1722	0.27	Aliased

Table 9 Model summary statistics for weld resistance length

Source	SD	R^2	Adjusted R^2	Predicted R^2	PRESS	
Linear	0.10	0.7357	0.6917	0.6071	0.37	
2FI	0.10	0.7931	0.6781	0.4911	0.48	
Quadratic	0.073	0.9200	0.8401	0.6983	0.28	Suggested
Cubic	0.083	0.9558	0.7937		+	Aliased

+ Case(s) with leverage of 1.00: PRESS statistic is not defined

model used with response surface designs is typically a second degree model with second-order interactions [14] as given below:

$$y = b_0 + \sum_{i=1}^{k} b_i \chi_i + \sum_{i=1}^{k} b_{ii} \chi_i^2 + \sum_{i<j} \sum_{j=2}^{k} b_{ii} \chi_i \chi_j + \varepsilon \qquad (2)$$

where, $b_{i,j}$=0,1,……k are called the regression coefficients, and ε is usually treated as a statistical error, which is often assumed to be independent with $N(0, \sigma^2)$ distributions.

2.3 Experimental design

A four-factor five-level central composite rotatable experimental design with full replication was planned to conduct the experiments. The statistical software Design-Expert V7 was used to create the design matrix and analyze the experimental data. The laser welding input variables are laser power (P), welding speed (S), angle of incidence (A), and defocus distance (D). In order to find the range of each process input parameter, initial trial runs were carried out by changing one of the process parameters while keeping the rest of them at constant values. The weld quality requirements stated in ISO 13919-1, i.e., absence of visible defects, size and position of weld spatter, and smooth appearance of welded surface were the selection criteria for the working range of each input factor. Table 2 shows primary input factors, their corresponding coded and actual levels, and response factors considered.

RSM was applied to the experimental data using the same software to develop mathematical models relating the selected welding parameters to each of the four output responses of the weld (weld penetration depth, radial penetration, resistance length, and shearing force). The adequacies of the models developed and their significant terms were measured by analyzing variance and other adequacy measures. Finally, these mathematical models were used to determine the optimal settings of welding parameters to ensure the desired weld quality. In this study, the quality criteria defined for the weld to determine the optimal settings of welding parameters are the minimization of weld radial penetration and the maximization of weld resistance length and shearing force. These optimization criteria were derived from mechanical and geometric requirements of fillet weld joint stated in ISO 15614-11.

2.4 Experimental work

Thirty experimental runs are carried out according to the design matrix in a random order to avoid any systematic error creeping into the system. Specimens were welded circularly in a fillet joint configuration using a 1.1 kW continuous wave Nd/YAG laser (Rofin DY011). During experimentation, laser power, welding speed, defocus distance, and incident angle are varied in the range 800–1,100 W, 4.5–7.5 m/min, −1.5 − +1.5 mm, and 10°–30°, respectively. The optical system consisted of a 300-μm fiber

Table 8 Sequential model sum of squares for weld resistance length

Source	Sum of squares	*df*	Mean square	*F* value	*p* Value prob>*F*	
Mean	34.48	1	34.48			
Linear	0.69	4	0.170	16.70	<0.0001	
2FI	0.054	6	0.009	0.83	0.5613	
Quadratic	0.12	4	0.030	5.56	0.0068	Suggested
Cubic	0.034	8	0.004	0.61	0.7493	Aliased

Table 10 Sequential model sum of squares for weld shearing force

Source	Sum of squares	*df*	Mean square	*F* value	*p* Value Prob>*F*	
Mean	4.34×10^{-6}	1	4.34×10^{-6}			
Linear	7.92×10^{-9}	4	1.98×10^{-9}	23.63	<0.0001	
2FI	5.68×10^{-10}	6	9.46×10^{-11}	1.18	0.3593	
Quadratic	7.15×10^{-10}	4	1.79×10^{-10}	3.30	0.0395	Suggested
Cubic	2.78×10^{-10}	8	3.47×10^{-11}	0.45	0.8542	Aliased

Table 11 Model summary statistics for weld shearing force

Source	SD	R^2	Adjusted R^2	Predicted R^2	PRESS	
Linear	9.15×10^{-6}	0.7908	0.7574	0.6975	3.03×10^{-9}	
2FI	8.96×10^{-6}	0.8475	0.7673	0.6916	3.09×10^{-9}	
Quadratic	7.36×10^{-6}	0.9190	0.8433	0.7080	2.92×10^{-9}	Suggested
Cubic	8.74×10^{-6}	0.9467	0.7790	0.7112	1.91×10^{-8}	Aliased

and two lenses of 200 mm focal and collimated lengths was able to deliver the laser with a minimum focal spot diameter of 300 μm. Argon is used as shielding gas with constant flow rate of 29 l/min to protect heated surface from oxidation and suppress plasma during welding. A standard washing procedure practised in the automotive industries is followed to clean, cool, and dry the specimens. None of the samples are subjected to any form of heat treatment after laser welding. However, the inner tube is made annealed prior to welding. Photographic views of the experimental setup for laser welding and push out test have been shown in Figs. 2 and 3, respectively

2.5 Mechanical characterization

After welding, each of specimens was first visually inspected and then cut axially to obtain transverse section of the welds under various welding conditions. Finally, part of the cut surfaces was prepared for metallographic inspection by polishing and etching to display a bead shape. The bead geometry was measured using an optical microscope (Leica MZ125) with an image analysis system (Leica IM500). Three pairs of coaxially assembled parts were welded for each combination of laser welding parameters to ensure statistical accuracy. The average value of each of the measured response factors was determined and recorded for further analyses. Push out tests were conducted to measure the shearing strength of the weld.

Push out tests were accomplished at room temperature (22.1°C) using Instron push-out calibrated press (model 3367) to determine the shearing load to failure of the welds fabricated under various conditions. During shearing test, specimens were set on a specimen holder or vice and pushed axially by a specially designed expeller so that the specimen fails due to shear along the resistance section of the weld as shown in Fig. 3. Table 3 shows the design matrix with actual factors and measured mean responses.

2.6 Optimization procedure

The optimization part in Design-Expert software V7 searches for a combination of factor levels that simultaneously satisfy the requirements placed (i.e., optimization criteria) on each of the responses and process input factors (i.e., multiple response optimization). Numerical and graphical optimization methods are used in this work by selecting the desired goals for each factor and response. The numerical optimization process involves combining the goals into an overall desirability function (D). The numerical optimization feature in the Design-Expert package finds one point or more in the factors domain that maximizes this objective function. In a graphical optimization with multiple responses, the software defines regions where requirements simultaneously meet the proposed criteria. Also, superimposing or overlaying critical response contours can be defined on a contour plot. Then, a visual search for the best compromise becomes possible. The graphical optimization displays the area of feasible response values in the factor space. Regions that fit the optimization criteria are colored [22]. Figure 4 shows flow chart of the optimization steps as developed [14].

Table 12 ANOVA table for weld penetration depth reduced quadratic model

Source	Sum of squares	*df*	Mean square	*F* value	*p* Value prob>*F*	
Model	1.090	7	0.160	277.72	<0.0001	significant
P (W)	0.570	1	0.570	1008.28	<0.0001	
S (m/min)	0.280	1	0.280	496.82	<0.0001	
A (degrees)	0.026	1	0.026	46.37	<0.0001	
D (mm)	0.0006	1	0.0006	1.07	0.3122	
A×D	0.045	1	0.045	79.76	<0.0001	
A^2	0.065	1	0.065	115.94	<0.0001	
D^2	0.130	1	0.130	228.09	<0.0001	
Residual	0.012	22	0.0006			
Cor total	1.10	29				
R^2=0.989	Adjusted R^2=0.985		Predicted R^2=0.981		Adq. precision=62.46	

Table 13 ANOVA table for weld radial penetration reduced quadratic model

Source	Sum of squares	*df*	Mean square	*F* value	*p* Value prob>F	
Model	0.310	7	0.044	64.43	<0.0001	significant
P (W)	0.069	1	0.069	101.08	<0.0001	
S (m/min)	0.038	1	0.038	55.69	<0.0001	
A (degrees)	0.160	1	0.16	233.60	<0.0001	
D (mm)	0.0007	1	0.0007	1.03	0.3213	
A×D	0.0071	1	0.0071	10.32	0.0040	
A^2	0.0031	1	0.0031	4.50	0.0453	
D^2	0.028	1	0.028	41.19	<0.0001	
Residual	0.015	22	0.0006			
Cor total	0.32	29				
R^2=0.954	Adjusted R^2=0.939		Predicted R^2=0.927		Adq. precision=30.84	

3 Results and discussion

3.1 Development of mathematical models

At this stage, the fit summary in the Design-Expert software is used to select the models that best describe the response factors. The fit summary includes sequential model sum squares to select the highest order polynomial where additional terms are significant and the model is not aliased. In addition, model summary statistics of the fit summary focuses on the model that maximizes adjusted R^2 and predicted R^2 values. The sequential *F* test and lack-of-fit test are carried out using the same statistical software package to check if the regression model is significant and to find out the significant model terms of the developed models as well. The step-wise regression method is also applied to eliminate the insignificant model terms automatically.

3.1.1 Response model selection

Suitable response models for the response factors are selected based on the fit summaries. From fit summary output of the measured responses shown in Tables 4, 5, 6, 7, 8, 9, 10, and 11, it is evident that quadratic model shown in Eq. 2 is statistically fitted to the experimental data to obtain the regression equations for all responses and can, therefore, be used for further analysis.

3.1.2 Analysis of variance

The test for significance of the regression models and the test for significance on individual model coefficients are performed using the same statistical package. By selecting the step-wise regression method that eliminates the insignificant model terms automatically, the resulting analysis of variance (ANOVA), Tables 12, 13, 14, and 15 for the selected models summarize the analysis of variance of each response and illustrate its significant model terms as well. The aforestated tables demonstrate that calculated Fisher's "Model *F*" and "Model *P*" values are, respectively, 277.72 and <0.0001 for weld penetration depth model, 64.43 and <0.0001 for radial penetration model, 34.55 and <0.0001 for weld resistance length model, and 28.42 and <0.0001 for weld shearing force model. These "Model *F*" and "Model *P*" values imply that the selected models are highly significant and there is only a less than 0.01% chance that these large "Model *F*" values could occur due to noise. The associated *P* values of less than 0.05 for the models (i.e., α=0.05 or 95% confidence level) indicate that the models are statistically significant as stated in [23]. The lack-of-fit values of the selected models given in Table 16

Table 14 ANOVA table for weld resistance length reduced quadratic model

Source	Sum of squares	*df*	Mean square	*F* value	*p* Value prob>*F*	
Model	0.83	5	0.17	34.55	<0.0001	Significant
P (W)	0.41	1	0.41	84.15	<0.0001	
S (m/min)	0.16	1	0.16	32.40	<0.0001	
A (°)	0.20	1	0.20	41.60	<0.0001	
P×A	0.036	1	0.036	7.37	0.0123	
A^2	0.11	1	0.11	22.73	<0.0001	
Residual	0.11	23	0.00482			
Cor total	0.94	28				
R^2=0.882	Adj. R^2=0.857		Pred. R^2=0.841		Adq. precision=20.13	

Table 15 ANOVA for weld shearing force reduced quadratic model

Source	Sum of squares	*df*	Mean square	*F* value	*p* Value prob>*F*	
Model	8.57×10^{-9}	5	1.71×10^{-9}	28.42	<0.0001	Significant
P (W)	3.41×10^{-9}	1	3.40×10^{-9}	56.50	<0.0001	
S (m/min)	2.84×10^{-9}	1	2.81×10^{-9}	47.13	<0.0001	
A (degrees)	1.58×10^{-9}	1	1.57×10^{-9}	26.14	<0.0001	
P×A	2.01×10^{-10}	1	2.01×10^{-10}	3.34	0.0801	
A^2	5.43×10^{-10}	1	5.42×10^{-10}	9.01	0.0062	
Residual	1.45×10^{-9}	24	6.03×10^{-11}			
Cor total	1.00×10^{-8}	29				
R^2=0.856	Adj. R^2=0.825		Pred. R^2=0.791		Adq. precision=18.34	

indicate nonsignificance, as it is desirable. Also, lack-of-fit *F* values imply that lack-of-fits are not significant relative to pure error.

The same ANOVA tables show the other adequacy measures, e.g., R^2, adjusted R^2, and predicted R^2 values. All these measures are in logical agreement and indicate significant relationships. Moreover, adequate precision compares range of predicted value at the design points to average prediction error. The adequate precision ratios in all cases are dramatically greater than 4 indicating adequate models discrimination.

From Tables 12 and 13 showing the ANOVA results for reduced quadratic models, it is evident that the main effects of *P*, *S*, and *A*, the quadratic effects of incident angle (A^2), and defocus distance (D^2) along with the interaction effects of incident angle and defocus distance ($A\times D$) are the significant model terms associated with weld penetration depth and radial penetration. Nevertheless, the effect of *D* is added to the aforestated models to support hierarchy. For the weld resistance length- and shearing force-reduced quadratic models, the corresponding ANOVA tables show that the main effects of *P*, *S*, and *A*, the quadratic effect of A^2 along with two-factor interaction of laser power and incident angle ($P\times A$) are the significant model terms. The other model terms are not significant and thus eliminated by backward elimination process to improve the model adequacy.

The developed statistical models are, therefore, fairly accurate and can be used for prediction within the same design space. The final models as determined by Design-Expert software are given below:

1. in terms of coded factors:

(a) Weld penetration depth

$$D_p = 1.25 + 0.31P - 0.22S - 0.066A + 1\times10^{-2}D - 0.21A\times D - 0.19A^2 - 0.27D^2 \quad (3)$$

(b) Weld radial penetration

$$P_r = 0.28 + 0.11P - 0.08S + 0.16A - 0.011D - 0.084A\times D + 0.042A^2 - 0.13D^2 \quad (4)$$

Table 16 Lack-of-fit tests for the selected models

	Sum of squares	*df*	Mean square	*F* value	*p* Value prob>*F*	
For weld penetration depth reduced quadratic model						
Lack of fit	0.0092	17	0.0005	0.86	0.6304	Not significant
Pure error	0.0031	5	0.0006			
For weld radial penetration reduced quadratic model						
Lack of fit	0.0057	17	0.0003	0.18	0.9967	Not significant
Pure error	0.0093	5	0.0019			
For weld resistance length reduced quadratic model						
Lack of fit	0.071	18	0.0039	0.50	0.874	Not significant
Pure error	0.040	5	0.0079			
For weld shearing force reduced quadratic model						
Lack of fit	1.04×10^{-9}	19	5.48×10^{-11}	0.68	0.757	Not significant
Pure error	4.05×10^{-10}	5	8.11×10^{-11}			

(c) Weld resistance length

$$S_L = 1.14 + 0.26P - 0.16S - 0.21A - 0.19P \times A - 0.33A^2 \quad (5)$$

(b) Weld shearing force

$$(F_s)^{-0.77} = 3.77 \times 10^{-4} - 2.383 \times 10^{-5}P + 2.176 \times 10^{-5}S + 1.621 \times 10^{-5}A + 1.419 \times 10^{-5}P \times A + 1.737 \times 10^{-5}A^2 \quad (6)$$

2. in terms of actual factors:

(a) Weld penetration depth

$$D_p = 0.0313 + 1.535 \times 10^{-3}P - 0.2155S + 0.0699A + 0.2887D - 0.0141A \times D - 1.9125 \times 10^{-3}A^2 - 0.1192D^2 \quad (7)$$

(b) Weld radial penetration

$$P_r = -0.0724 + 5.3667 \times 10^{-4}P - 0.0797S - 3.333 \times 10^{-4}A + 0.1048D - 5.6 \times 10^{-3}A \times D + 4.1625 \times 10^{-4}A^2 - 0.0559D^2 \quad (8)$$

(c) Weld resistance length

$$S_L = -1.8191 + 3.185 \times 10^{-3}P - 0.1613S + 0.1864A - 9.425 \times 10^{-5}P \times A - 3.31 \times 10^{-3}A^2 \quad (9)$$

(d) Weld shearing force

$$(F_s)^{-0.77} = 5.577 \times 10^{-4} - 2.61 \times 10^{-7}P + 2.176 \times 10^{-5}S - 1.1 \times 10^{-5}A + 7.093 \times 10^{-9}P \times A + 1.737 \times 10^{-7}A^2 \quad (10)$$

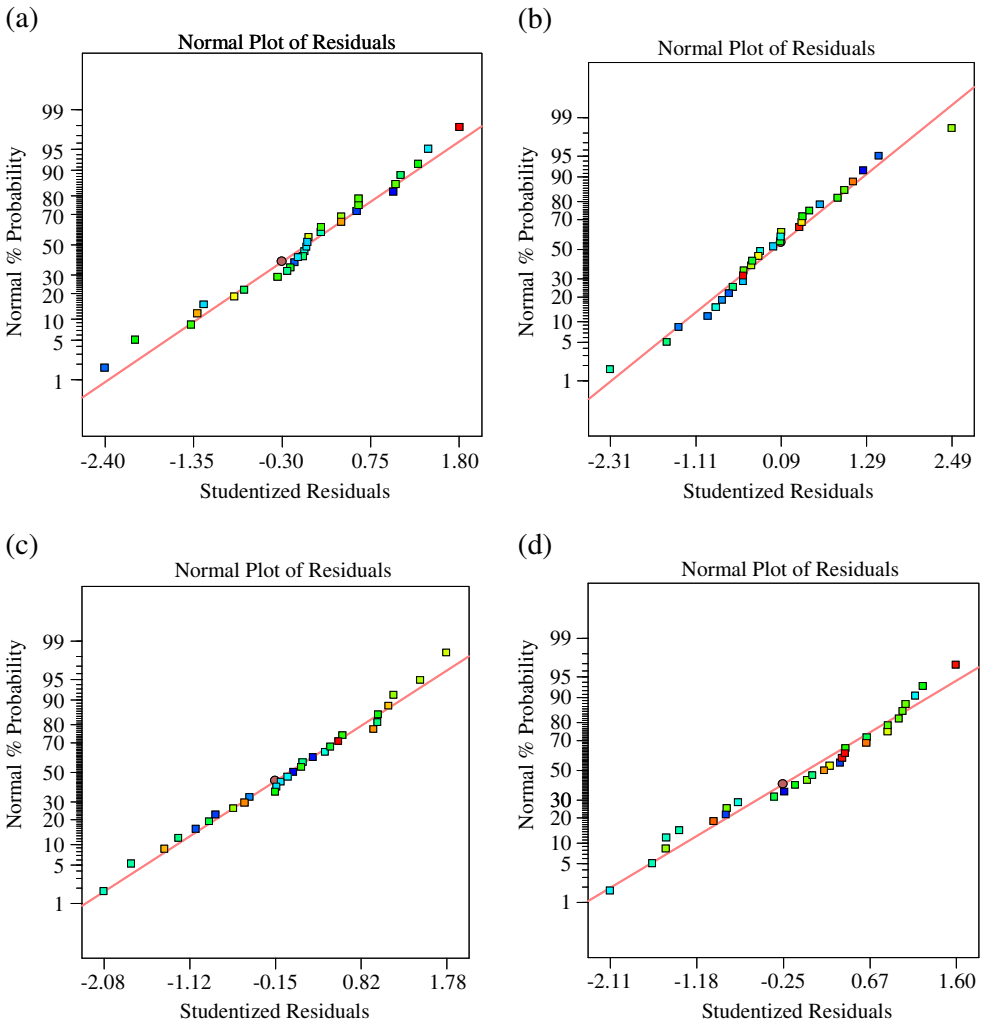

Fig. 5 Normal probability plot for weld **a** penetration depth, **b** radial penetration, **c** resistance length, and **d** shearing force

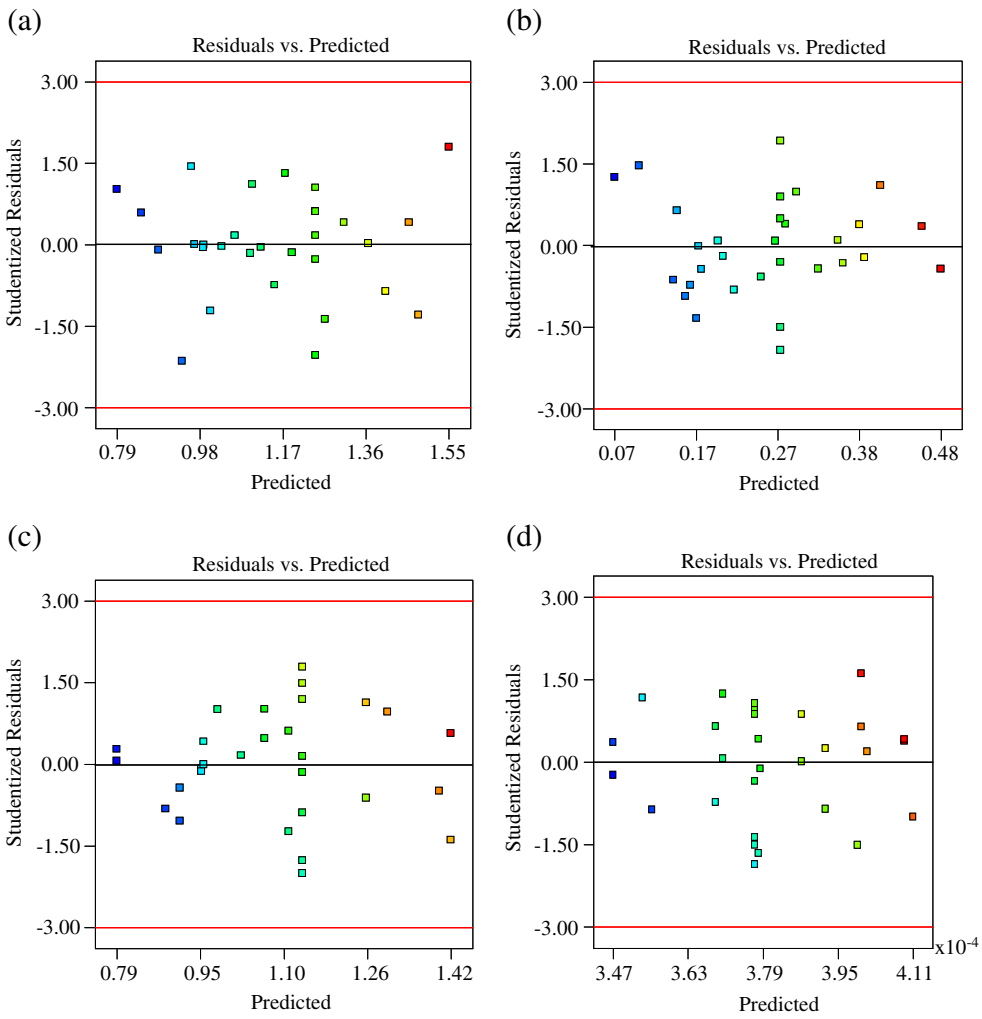

Fig. 6 Studentized residual vs. predicted plot for weld **a** penetration depth, **b** radial penetration, **c** resistance length, and **d** shearing force

3.1.3 Validation of developed model

Normality of residual data, pattern of error variance, presence of outliers, and amount of residuals in prediction are checked to ensure statistical validation of the developed models. The normality of data is verified by plotting the normal probability plot of residuals. The residual is the difference between observed and predicted value (or fitted value) obtained from the regression model. The data set is normally distributed if the points on the plot fall fairly close to the straight line. The normal probability plots of residual values for weld penetration depth, radial penetration, resistance length, and shearing force are illustrated in Fig. 5a–d, respectively. The experimental points are reasonably aligned with predicted or fitted points suggesting the normality of data.

Figure 6a–d demonstrate studentized residuals versus fitted values (predicted response) for weld penetration. The residuals are found to be scattered randomly about zero. This indicates that errors have a constant variance for all response variables. Plot of standardized residuals versus predicted values also shows the possible existence of outliers. If a point lies far from the majority of points, it may be an outlier. It is important to identify the outliers as these can significantly influence the model and provide potentially misleading or incorrect results. As shown in the figures, all the points are within ±2.0σ limits for each of the response models and confirm no existence of such outliers.

Figure 7a–d are showing the relationships between the actual and predicted values of weld penetration depth, radial penetration, resistance length, and shearing forces, respectively. These figures illustrate that the developed models are adequate and predicted results are in good agreement with the measured data as the residuals are close to the diagonal line.

Besides, three confirmation experiments are conducted with welding conditions chosen randomly within the ranges for which the equations are developed in order to validate the developed response surface equations derived from multiple regression analyses. The actual results are calculated as the average of three measured results for each response. The actual results, predicted values, and calculated percentage error of confirmation experiments are

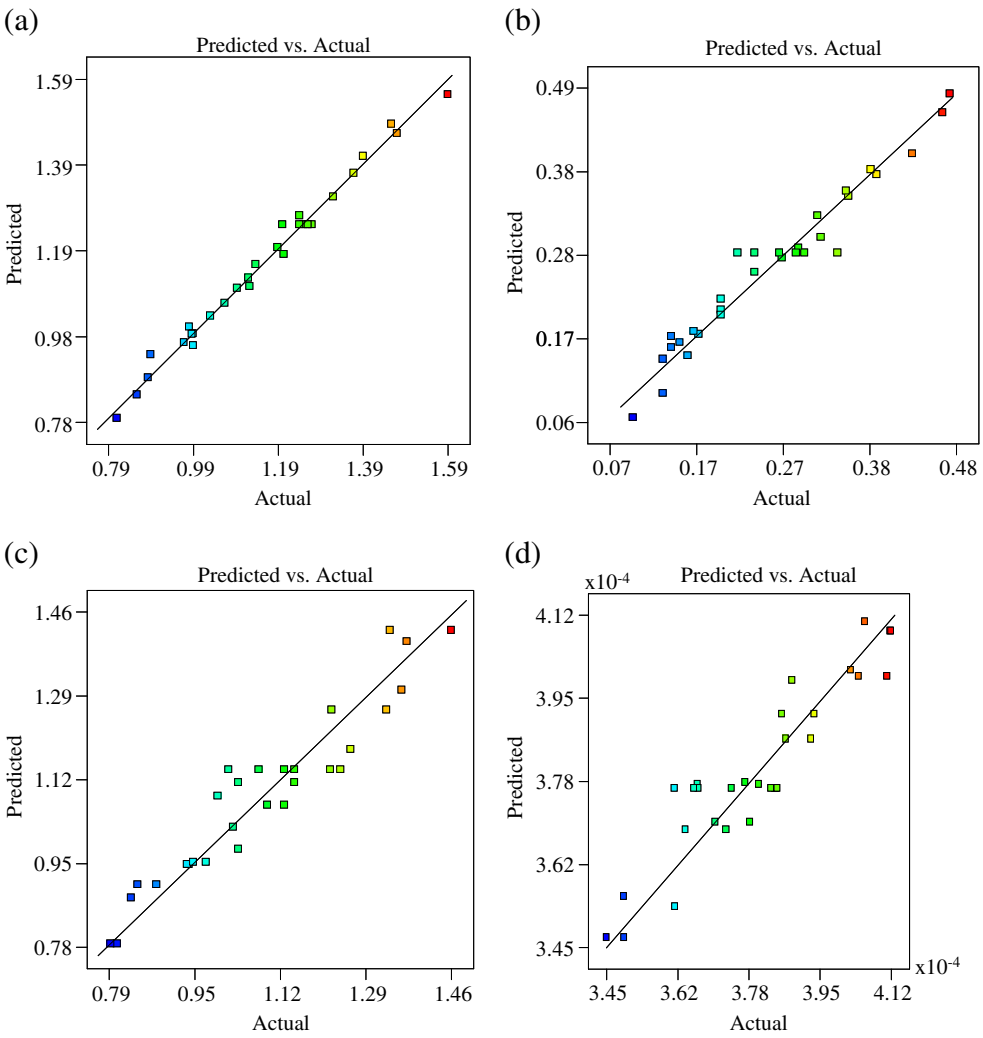

Fig. 7 Scatter diagrams of weld **a** penetration depth, **b** radial penetration, **c** resistance length, and **d** shearing force

given in Table 17. It is observed from the validation experiments that there is a small percentage error between the estimated and the experimental values. These results indicate that the developed models can yield nearly accurate results.

3.2 Effect of line energy (*P*/*S*) on weld bead characteristics

The energy delivered per unit length of weld line is referred to as line energy (LE), which is frequently used in various laser processing techniques and termed as a key parameter

Table 17 Confirmation experiments

No. of expt	Process parameters					Response factors			
	P (W)	*S* (m/min)	*A* (degrees)	*D* (mm)		P_r (mm)	D_P (mm)	S_L (mm)	F_S (*N*)
Expt. I	950	3.0	25	0.75	Actual	0.390	1.260	1.110	28,890
					Predicted	0.392	1.281	1.075	27,946
					Error(%)	0.517	1.53	−3.12	−3.39
Expt. II	850	3	15	−0.75	Actual	0.185	1.155	1.285	29,390
					Predicted	0.186	1.183	1.253	29,082
					Error(%)	0.062	2.41	−2.47	−1.05
Expt. III	750	2.0	20	0	Actual	0.328	1.355	1.280	30,770
					Predicted	0.331	1.385	1.236	29,534
					Error (%)	0.912	2.24	−3.51	−4.19

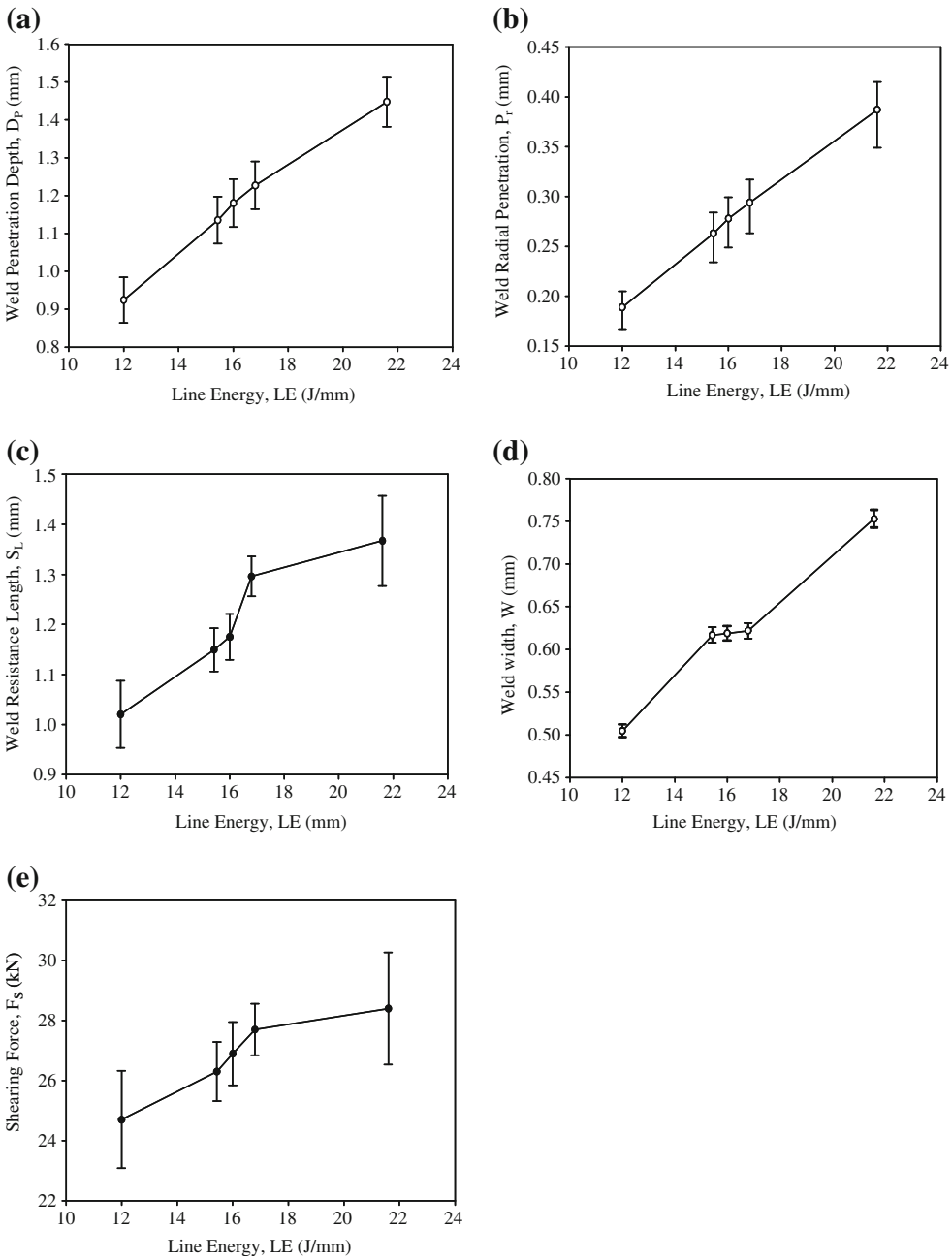

Fig. 8 Effect of line energy on weld **a** penetration depth, **b** radial penetration, **c** resistance length **d** width and **e** shearing force for A=15° and D=0.0 mm

when continuous-wave laser is used. This term is calculated as the ratio of laser power over the welding speed as shown in Eq. 1:

$$\mathrm{LE} = 0.06 \times \frac{P}{S}(kJ/m) \tag{1}$$

Where, LE is line energy, P is laser power in Watt (W) describing the thermal source, and S is welding speed in meter per minute determining the irradiation time. According to the Eq. 1, the combinations of laser power of 600–1,000 W and welding speed of 2.0–4.0 m/min resulted in nominal line energy input in the range of 12.0–24.0 kJ/m.

In this section, different weld bead characteristics, i.e., weld width; penetration depth, radial penetration, resistance length, and shearing force are plotted against the line energy keeping the angle of incidence and defocus distance constant at a particular value. Variation of weld form factor, i.e., width-to-penetration depth ratio with the line energy input has also been illustrated. The objectives of plotting these graphs are of twofold:

- showing the effects of line energy input on weld profile characteristics, and
- explaining different laser welding phenomena.

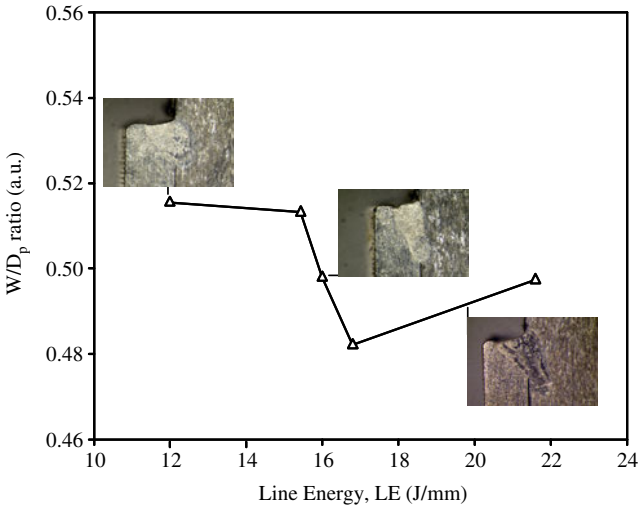

Fig. 9 Effect of line energy on weld shape factor for A=15° and D= 0.0 mm

Figure 8a–e show the effects of line energy input on the weld penetration depth (D_P), radial penetration (P_r), resistance length (S_L), width (W), and shearing force (F_S), respectively, while variation of width-to-penetration depth (W/D_P) with line energy input has been illustrated in Fig. 9.

From Fig. 8a and b, it is found that both the weld penetration depth and radial penetration depth increases with the line energy input for a fixed laser beam incident angle. Increasing line energy input to the weld area results in greater volume of materials being melted with a consequent increase in weld penetration depth and hence, the larger weld radial penetration shown in Fig. 1 is achieved.

Again, Fig. 8c–d show that both the weld resistance length and the width grow positively with the increase in line energy input up to a certain level. After that level, almost no change in weld width and a rapid increase in weld resistance length are observed for the line energy in the range of 15–17 kJ/m. These are because of the change in welding modes from conduction-limited to keyhole with increase in the line energy input from 12 to 17 kJ/m. Besides, as illustrated in Fig. 8e, variation in weld shearing force with the energy input follows the same pattern as the weld resistance length. This is because of the existing linear, positive relationship between them as stated in [24]

For line energy in the range of 12–15 kJ/m, as illustrated in Figs. 8d and 9, there is a rapid increase in W with energy input, whereas reduction in weld shape factor, i.e., width-to-penetration depth ratio (W/D_p) is negligible. Slight negative variations of this factor prove that the laser welding is mainly conduction limited. Since the melt pool geometry depends on energy intensity, uniform conduction occurring in all directions usually results in semicircular weld profile. However, the heat conduction along the beam axis becomes dominant with the increase in energy input and weld shape changes from semicircular to parabolic.

A sharp reduction (starting from 15 kJ/m) in weld shape factor for the line energy in the range of 15–17 kJ/m demonstrates the fact that the weld penetration depth increases at a faster rate than the weld width in this range and establishes a keyhole formation regime. As a result, the weld bead becomes almost cylindrical. W/D_P ratio is found to rise with further increase in line energy. This is because of the creation of upper keyhole plasma plume that acts as a point heat source above weld plane.

3.3 Process parameter optimization

From weld design specification as described in ISO15614-11, weld radial penetration, resistance length, and shearing force are the response factors that characterize a fillet welded joint. Laser fillet welding input parameters should be optimized to obtain the optimal values of these response factors. Two sets of criteria have been implemented in

Table 18 Optimization criteria used in this study

Name	Limit		First criterion		Second criterion	
	Lower	Upper	Goal	Importance	Goal	Importance
P (W)	600	1,000	Is in range	3	Minimize	5
S (m/min)	2	4	Is in range	3	Maximize	5
A (degrees)	10	30	Is in range	3	Minimize	5
D (mm)	−1.5	1.5	Is in range	3	Is target=0	5
S_L (mm)	0.790	1.457	Maximize	5	Maximize	5
P_r (mm)	0.094	0.475	Minimize	5	Minimize	5
F_s (N)	24,933	31,317	Maximize	5	Maximize	5

Table 19 Optimal solutions as obtained based on first criterion

Sol^n no.	P (W)	S (m/min)	A (degree)	D (mm)	S_L (mm)	P_r (mm)	F_s (N)
1	1,000	3.24	10.4	0.00	1.444	0.248	31,317
2	1,000	3.24	10.3	0.00	1.440	0.247	31,317
3	1,000	3.24	10.6	0.00	1.440	0.249	31,317
4	1,000	3.24	10.2	0.00	1.438	0.246	31,317
5	1,000	3.25	10.8	0.00	1.451	0.251	31,317
6	1,000	3.23	10.0	0.00	1.434	0.245	31,317
7	999	3.23	10.4	0.00	1.441	0.248	31,317
8	1,000	3.21	10.3	0.00	1.444	0.249	31,386
9	1,000	3.20	10.0	0.00	1.447	0.245	31,410

the numerical optimization. The first set of criteria is to reach minimum radial penetration, and maximum resistance length and shearing force of the weld with no limitation on the process parameters. For this particular type of joint, lowering the laser power and incident angle, and increasing the welding speed are the most common techniques used in automotive industries to produce relatively low cost and excellent weld joints. Taking these cost and quality aspects into account, the second set of criteria are fixed to maximize welding speed and minimize laser power and incident angle along with the goals defined for the response factors in the first set. Also, a target value of zero is set to defocus distance as the focused beam (D=0 mm) provides the smallest spot diameter on the weld plane and hence, the highest energy input onto the materials being welded. Table 18 summarizes these two criteria, limiting values and importance for each input and response factor.

Tables 19 and 20 show the optimal solutions based on two optimization criteria as determined by Design-Expert software. The results demonstrate that, whatever the criteria, the laser has to be focused on the weld plane (i.e., D=0 mm) to obtain a weld with longer resistance length, smaller radial penetration, and higher shearing force.

Again, from Table 19, demonstrating the optimal welding conditions based on the first set of criteria, it is evident that the obtainable longest resistance length, the smallest radial penetration and the highest shearing force are respectively 1.447 mm, 0.245 mm, and 31,410 N for laser power, welding speed and incident angle of 1,000 W, 3.2 m/min and 10°, respectively. However, with an acceptable weld resistance length, radial penetration, and shearing force, the laser power can be minimized to 865 W, and the welding speed can be maximized to 4 m/min as shown in Table 20. However, incident angle increases to 12°. Under this condition, the weld penetration depth, resistance length and shearing force are found to be 1.176 mm, 0.18 mm, and 28,479 N, respectively, which are much greater than the respective prerequisite values for this particular weld.

The aforestated tables also show that, for the first set of optimization criteria, the optimal range of welding speed is 3.2–3.25 m/min with a laser power of 1,000 W. However, the optimal ranges of laser power and welding speed can be reduced to 860–875 W and increased to 3.4–4.0 m/min, respectively, if the second set of optimization criteria are applied. As a consequence, any combination of process

Table 20 Optimal solutions as obtained based on second criterion

Sol^n no.	P (W)	S (m/min)	A (degree)	D (mm)	S_L (mm)	P_r (mm)	F_s (N)
1	875	3.44	11.7	0.00	1.177	0.177	28,468
2	874	3.43	11.7	0.00	1.178	0.177	28,479
3	876	3.45	11.7	0.00	1.179	0.177	28,473
4	877	3.45	11.7	0.00	1.176	0.176	28,455
5	875	3.43	11.8	0.00	1.180	0.178	28,484
6	877	3.44	11.6	0.00	1.179	0.176	28,493
7	873	3.44	11.8	0.00	1.176	0.176	28,433
8	865	4.00	12.0	0.00	1.176	0.180	28,479

Table 21 Visual inspection of weld quality

Process parameters				Visual check		
P (W)	*S* (m/min)	*A* (degree)	*D* (mm)	Spatter	Cracks	Blow holes
700	2.5	15	−0.75	1	0	0
900	2.5	15	−0.75	1	1	0
700	3.5	15	0.75	0	0	0
900	3.5	15	0.75	1	1	0
800	3.0	10	0	1	1	0
800	3.0	30	0	1	0	0
800	2.0	20	0	1	1	0
800	4.0	20	0	0	0	0
600	3.0	20	0	0	0	0
1,000	3.0	20	0	2	0	1

0 no defect, *1* marginally acceptable, *2* not acceptable

parameters for the second optimal settings would cause less energy density input to the weld. The reduced energy input that results in less distortion and formation of cracks, blow holes, and spatter would lead to better weld quality as can be seen from visual inspection data given in Table 21.

Moreover, the graphical optimization allows visual selection of the optimum welding conditions according to certain criterion. The result of the graphical optimization are the overlay plots and these type of plots are extremely practical for quick technical use in the workshop to choose the values of the welding parameters that would achieve certain response value for this type of material. The yellow-colored areas on the overlay plots shown in Fig. 10a and b are the regions that meet the proposed criteria.

4 Conclusion

For the laser system, weld joint type and the limits of laser parameters considered in this study, the following points can be concluded:

1. RSM is an accurate technique to optimize the laser welding process in order to obtain the most desirable weld quality in terms of weld bead geometry and mechanical strength, and to determine the corresponding optimal settings of welding parameters.
2. Laser power, welding speed, and angle of incidence are the most significant factors that affect the weld bead geometry and shearing force. Interactions of beam incident angle with laser power and defocus distance are also found to have substantial effects on the weld bead characteristics.
3. A sharp decrease in weld shape factor and increase in shearing force with the line energy input in the range of 15–17 kJ/m depicts the establishment of a keyhole regime.
4. Laser power and welding speed of a focused beam in the range 860–875 W and 3.4–4.0 m/min, respectively, with an incident angle of around 12° are the optimal settings of fillet welding input parameters to obtain an excellent welded component made of ferritic AISI 430 and austenitic AISI 304L stainless steels.
5. Weld joint of desired quality and strength could be using the optimal welding combinations obtained from the numerical optimization.
6. The graphical optimization results allows quicker search for the optimal settings for laser fillet welding.

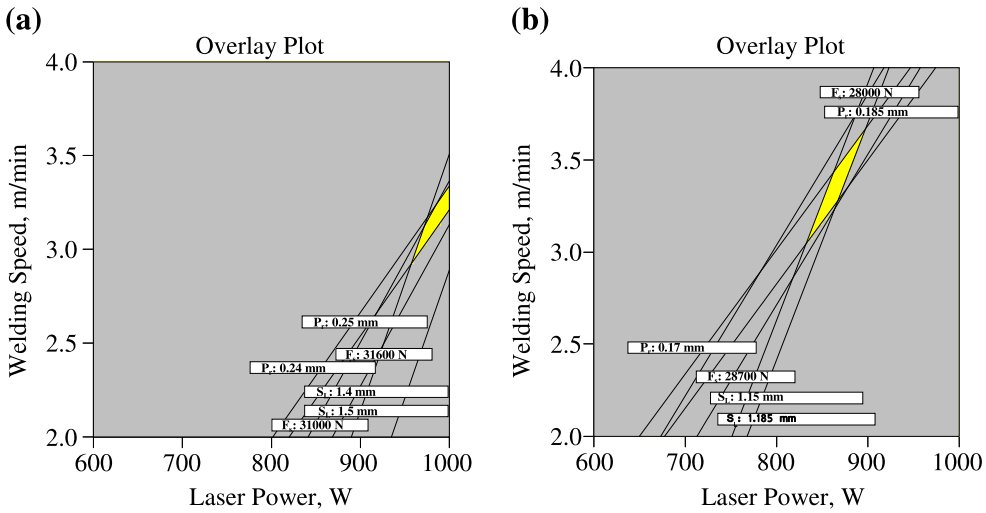

Fig. 10 Overlay plots show the region of optimal welding condition based on **a** the first criterion at $A=10°$ and $D=0$ and **b** the second criterion at $A=12°$ and $D=0$

Nomenclature

P	Laser power, W
S	Welding speed, m/min
A	Angle of incidence, degree
D	Defocus distance, mm
W	Weld width, mm
P_r	Weld radial penetration, mm
D_P	Weld penetration depth, mm
S_L	Weld resistance length, mm
F_s	Weld shearing force, N
LE	Line energy, kJ/mm
W/D_P	Weld shape factor, a.u.

References

1. Steem WM, Mazumder J (2010) Laser material processing. Springer, London
2. Weichiat C, Paul A, Pal M (2009) CO_2 laser welding of galvanized steel sheets using vent holes. Mater Des 30:245–251
3. Mackwood AP, Crafer RC (2005) Thermal modeling of laser welding and related processes: a literature review. Opt Laser Technol 37:99–115
4. Kaiser E, Schafer P (2005) Pulse shaping optimizes the quality of seam and spot welds. In: Lasers in manufacturing, Proceeding of The Third International WLT—Conference on Lasers in Manufacturing. pp. 695–670
5. Sun Z, Kuo M (1998) Bridging the joint gap with wire feed laser welding. J Mater Process Technol 87:213–222
6. Liu X-B, Yu G, Guo J, Gu Y-J, Pang M, Zheng C-Y, Wang H-H (2008) Research on laser welding of cast Ni-based superalloy K418 turbo disk and alloy steel 42CrMo shaft. J Alloy Comp 453(1–2):371–378
7. Huang Q, Hagstroem J, Skoog H, Kullberg G (1991) Effect of CO_2 laser parameter variations on sheet metal welding. Int J Join Mater 3(3):79–88
8. Juang SC, Tarng YS (2002) Process parameter selection for optimizing the weld pool geometry in the tungsten inert gas welding of stainless steel. J Mater Process Technol 122:33–37
9. Marya M, Edwards G, Marya S, Olson DL (2001) Fundamentals in the fusion welding of magnesium and its alloys. In: Proceedings of the Seventh JWS international Symposium. pp. 597–602
10. Haferkamp H, Niemeyer M, Dilthey U, Trager G (2000) Laser and electron beam welding of magnesium materials. Weld Cutt 52 (8):178–180
11. Haferkamp H, Bach Fr-W, Burmester I, Kreutzburg K, Niemeyer M (1996) Nd:YAG laser beam welding of magnesium constructions. In: Proceedings of the Third International Magnesium Conference. pp. 89–98
12. Benyounis KY, Olabi AG, Hashmi MSJ (2005) Effect of laser welding parameters on the heat input and weld-bead profile. J Mater Process Technol 164–165:978–985
13. Manonmani K, Murugan N, Buvanasekaran G (2007) Effects of process parameters on the bead geometry of laser beam butt welded stainless steel sheets. J Adv Manuf Technol 32(11–12):1125–1133
14. Benyounis KY, Olabi AG, Hashmi MSJ (2008) Multi-response optimization of CO_2 laser-welding process of austenitic stainless steel. Opt Laser Technol 40:76–87
15. Moradi M, Ghoreishi M (2010) Influences of laser welding parameters on the geometric profile of NI-base superalloy Rene 80 weld-bead. Int J Adv Manuf Technol. doi:10.1007/s00170-010-3036-1
16. Padmanaban G, Balasubramanian V (2010) Optimization of laser beam welding process parameters to attain maximum tensile strength in AZ31B magnesium alloy. Opt Laser Technol 42: 1253–1260
17. Rajakumar S, Muralidharan C, Balasubramanian V (2010) Optimization of the friction-stir-welding process and the tool parameters to attain a maximum tensile strength of AA7075-T6 aluminium alloy. J Eng Manuf 224:1175–1191
18. Ruggiero A, Tricarico L, Olabi AG, Benyounis KY (2011) Weld-bead profile and costs optimization of the CO_2 dissimilar laser welding process of low carbon steel and austenitic steel AISI316. Opt Laser Technol 43:82–90
19. Myers RH, Montgomery DC (2002) Response surface methodology: process and product optimization using designed experiments. Wiley, New York
20. Robinson TJ, Wulff SS (2006) Response surface approaches to robust parameter design. In: Khuri AI (ed) Response surface methodology and related topics. World Scientific, Singapore, pp 123–157
21. Gunaraj V, Murugan N (1999) Application of response surface methodologies for predicting weld base quality in submerged arc welding of pipes. J Mater Process Technol 88:266–275
22. Design-ExpertSoftware,V7 (2005) User's guide: technical manual. Stat-Ease Inc., Minneapolis
23. Zulkali MMD, Ahmad AL, Norulakmal NH (2006) *Oryza sativa* L. husk as heavy metal adsorbent: optimization with lead as model solution. Bioresour Technol 97:21–25
24. Cui C, Hu J, Gao K, Pang S, Yang Y, Wang H, Guo Z (2008) Effects of process parameters on weld metal keyhole characteristics with CO2 laser butt welding. Lasers Eng 18:319–327
25. Khan MMA, Romoli L, Fiaschi M, Sarri F, Dini G (2010) Experimental investigation on laser beam welding of martensitic stainless steels in a constrained overlap joint configuration. J Mater Process Technol 210:1340–1353